Lyman-α Spectroscopy of Magnetically Trapped Atomic Hydrogen

O. J. Luiten, H. G. C. Werij, I. D. Setija, M. W. Reynolds, T. W. Hijmans, and J. T. M. Walraven
Universiteit van Amsterdam, Van der Waals–Zeeman Laboratorium, Valckenierstraat 65/67, 1018 XE Amsterdam, The Netherlands
(Received 21 October 1992)

We describe the first optical experiments on atomic hydrogen in a magnetic trap, using a narrow-band source at Lyman-α wavelength. By means of transmission spectroscopy we have studied the temperature and density evolution of the gas during evaporative cooling in a fixed field geometry.

PACS numbers: 32.80.Pj, 07.65.Eh, 67.65.+z

Recent experiments with magnetically trapped atomic hydrogen have underlined the importance of combining the goals and concepts of spin-polarized hydrogen research with those of the field of neutral particle cooling and trapping [1–4]. Eliminating the influence of physical surfaces, gaseous samples may be studied under exceptionally well-defined conditions from the collisionless regime up to densities where it should be possible to observe the effects of quantum degeneracy. Thus far magnetically trapped H could only be studied by indirect methods based on the observation of atoms *after* they escape from the trap. This escape can be due to an intrinsic process, such as magnetic relaxation [2], or to deliberate lowering of a magnetic barrier, such as during forced evaporative cooling [3, 4]. Although these indirect methods are powerful, more direct methods, enabling *in situ* determination of temperature and density, are essential for further development of the field [5].

In this Letter we report the first *in situ* observation of magnetically trapped H by means of $1^2S \rightarrow 2^2P$ Lyman-α (L_α, $\lambda = 121.6\,\mathrm{nm}$) transmission spectroscopy. Spectroscopy (and optical cooling) of magnetostatically trapped Na was reported previously by Helmerson, Martia, and Pritchard [6]. We use transmission spectroscopy to investigate the temporal development of the temperature and density of H gas during evaporative cooling. An accurate description of the transmission spectrum allows us to determine spectroscopically the temperature and density of the trapped gas with an absolute accuracy of typically 25%. For our conditions a minimum of $\sim 5 \times 10^8$ atoms is required to record a complete transmission spectrum with unity signal-to-noise ratio within 30 s.

Because of the absence of a suitable cw light source in the vacuum ultraviolet (VUV), H cannot be manipulated with the same techniques developed to optically cool and trap other atoms, such as Na [6–8]. To trap hydrogen, Hess proposed to surround a static minimum-B-field trap by helium-covered walls, which thermalize the atoms into the trap [9]. In a typical experiment the H atoms are produced in a high field (4 T) in all four hyperfine states (labeled a, b, c, and d in order of increasing energy) by a low-temperature (~ 0.5 K) rf discharge. The atoms in the a and b states (H$\downarrow$) are removed through forced recombination on a helium-free bolometer surface; the atoms in the c and d states (H$\uparrow$) are pulled into the trapping region, from which they cannot escape due to the presence of the surrounding walls. After internal thermalization the gas temperature T relaxes to the wall temperature T_w. The c-state atoms rapidly disappear due to spin-exchange relaxation to H$\downarrow$ states [2, 10] and will be neglected henceforth. This cryogenic filling technique allows for the accumulation of relatively high densities, well suited for evaporative cooling and for the investigation of collisional phenomena [1–4].

For the present experiments the Ioffe trap used by van Roijen *et al.* [2] was modified to produce longer samples. A contour plot of the field configuration is shown in Fig. 1. The well depth of the trap $\epsilon_{\mathrm{tr}}/k_B = \mu_B(B_w - B_0)/k_B \approx 0.82\,\mathrm{K}$, where B_w and B_0 are the field at the side wall and at the trap minimum, respectively, and μ_B is the Bohr magneton. The density distribution in thermal equilibrium is given by $n(\mathbf{r}) = n_0 \exp[-U_p(\mathbf{r})/k_B T]$, where n_0 is the density at the center of the trap, and $U_p(\mathbf{r}) = \mu_B[B(\mathbf{r}) - B_0]$. The sample cell, made out of copper, is mounted inside the bore of the Ioffe trap and linked to the mixing chamber of a dilution refrigerator. Optical access is provided from below along the symmetry axis of the cryostat through an indium-sealed MgF_2

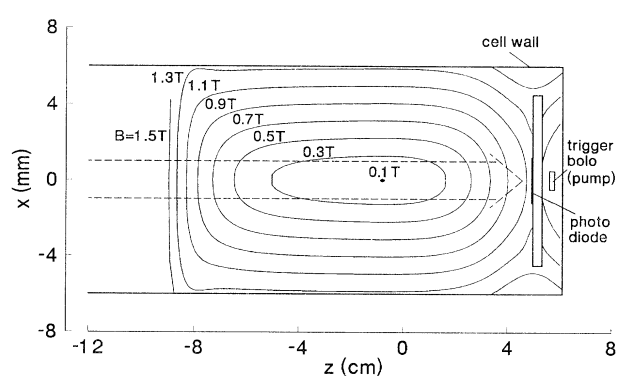

FIG. 1. Contour plot of the trapping field B in the experimental cell. The arrow indicates the L_α beam.

window at the bottom end of the cell. To measure the transmission of the light through the sample, a GaAsP Schottky photodiode is mounted at the upper end of the cell. The quantum efficiency of this detector for L_α is $\sim 10\%$ at 0.2 K in a field of 1.5 T. A MgF_2 beam splitter near the entrance of the cryostat enables a ratio measurement that strongly reduces the noise arising from the 10% pulse-to-pulse power fluctuations of the L_α source.

The L_α source is based on nonresonant third-harmonic generation of pulse-amplified 364.8 nm ultraviolet (UV) radiation, obtained by frequency doubling of (pulse-amplified) light from a tunable cw dye laser. Typically we produce 3×10^9 L_α photons per pulse, in 10 ns pulses at a repetition rate of 50 Hz. Only $\sim 2\%$ of the light arrives at the sample, primarily due to absorption losses in the MgF_2 components and the beam alignment optics. By properly choosing the plane of polarization of the linearly polarized UV light the helicity and ellipticity of the L_α beam can be selected, taking advantage of the birefringence of the optical components. The bandwidth of the VUV radiation ($\sim$ 150 MHz) is comparable to the natural linewidth of the L_α transitions (100 MHz). The spectrum can be recorded by sweeping the frequency of the cw laser. A chain of three acousto-optic modulators (AOM) enables pulse-to-pulse switching of the VUV frequency between -0.48 GHz, $+0.48$ GHz, and $+0.90$ GHz, relative to the sixth harmonic of the cw laser frequency. A detailed description of our L_α source is given elsewhere [5, 11].

We will first describe how we infer T and n_0 from transmission spectra. In Fig. 2 two typical transmission spectra are shown, taken with left- and right-handed circular polarization. Disregarding the hyperfine structure of the 2^2P states, three σ transitions and two π transitions are allowed in a pure d-state gas, denoted σ_1, σ_2, σ_3, π_1, and π_2 (see Fig. 2). The broadening of the lines is due to Doppler and Zeeman shifts. Because the Zeeman shifts (positive for σ_1, negative for the other transitions) are dominant for $T \gtrsim 20$ mK, the line shapes reflect the density distribution $n(\mathbf{r})$ in the trapping field $B(\mathbf{r})$, as is also the case in Ref. [6].

The interpretation of the measured transmission spectra is complicated by the fact that both the magnitude and direction of the field are nonuniform over the sample. Moreover, at densities $n_0 \gtrsim 10^{11}\,\mathrm{cm}^{-3}$, the sample can be optically thick, completely blocking the central part of the beam. Further, it turns out that under such conditions dispersion (Faraday effect) cannot be neglected and can change the transmission by as much as 40% in regions where π and σ lines overlap. To extract T and n_0, the measured data are compared with numerically calculated spectra. The calculation entails propagating the complex field amplitude through the sample using the known contributions of the five allowed transitions to the complex tensor susceptibility of the gas at each point in space. The beam shape is taken into account by appropriate weighing in the radial integration of the intensity. The calculation is performed for both left and right circularly polarized light. For a circular beam, a suitable linear combination of these two spectra, convoluted with the spectral function of the source, exactly represents the spectrum for arbitrary polarization. In Fig. 2 fits to the data are shown from which T and n_0 are obtained with $\sim 25\%$ accuracy, limited predominantly by imprecise knowledge of the beam shape.

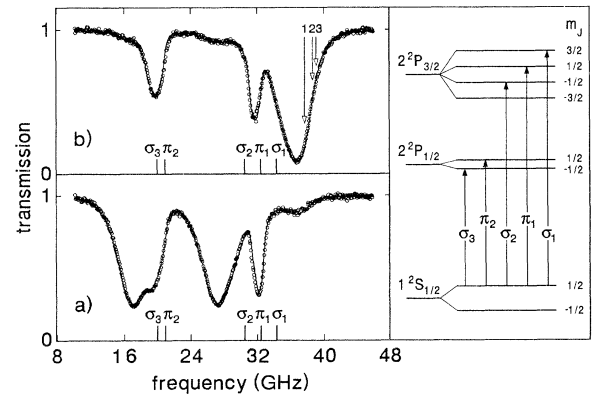

FIG. 2. Transmission spectra, recorded with (a) right- and (b) left-circularly polarized light, and energy level diagram defining the five allowed transitions. The scan time for each spectrum is 30 s. The solid lines are calculated spectra for $T = 51(12)$ mK and (a) $n_0 = 4.4(1.0) \times 10^{12}\,\mathrm{cm}^{-3}$ and (b) $n_0 = 3.3(0.8) \times 10^{12}\,\mathrm{cm}^{-3}$. The frequency is relative to $\frac{3}{4}R_\infty(1 + m_e/m_p)^{-1}$. The vertical bars denote the resonant frequencies of the five allowed transitions for $B = B_0$. The arrows in (b) indicate the three AOM frequencies.

To determine T and n_0 under transient conditions, i.e., on a time scale short in comparison to the time required for a full spectral scan, we record the L_α transmission P at three fixed frequencies ν in the blue wing of the σ_1 line using the acousto-optic modulator chain. To analyze the data we use the following form to describe the blue wing of this line:

$$\ln P = -\sigma_0\, n(\Delta\nu, T, n_0)\, \ell(\Delta\nu, T, n_0)\,. \tag{1}$$

Here $\sigma_0 = \lambda^2/2\pi$ and $\Delta\nu = \mu_B(B - B_0)/h$ is the detuning from the σ_1-resonance frequency at the trap minimum. The length ℓ is the effective axial distance over which the light is resonant with σ_1 and $n = n_0 \exp[-h\Delta\nu/k_B T]$ is the corresponding local density. Using the approximately quadratic z dependence of B, we can write $\ell = \ell_0[\Delta\nu_w/\Delta\nu]^{1/2}$, with $\Delta\nu_w$ the detuning for $B = B_w$, where ℓ_0 (≈ 1.6 mm) is a slowly varying function of $\Delta\nu$, T, and n_0, which is determined numerically. Details related to, e.g., Doppler broadening and the radial extent of the sample are lumped into ℓ_0. Equation (1) holds for left circularly polarized light. For arbitrary polarization, P should be appropriately transformed.

We now turn to a discussion of evaporative cooling.

In our system the evaporation is started *after* loading the trap and in a static field geometry. These experiments were done at the lowest attainable cell temperature, $T_w \approx 0.2\,\mathrm{K}$, limited by a spurious radiative heat load entering along the light path. To start the evaporation we energize a small bolometer which is mounted behind the photodiode, in high field, as shown in Fig. 1. By boiling off the He film, the bolometer surface acts as a sorption pump, removing high-energy H atoms, which leads to (evaporative) cooling of the remaining H gas. The photodiode housing acts as a baffle, which protects the H sample against evaporating He atoms. To illustrate the experimental procedure, we show in Fig. 3 the transmission versus time at the three frequencies indicated by arrows in Fig. 2. The data shown were taken on a single sample of trapped H↑ with an integration time of 80 ms (four pulses) per data point. The jump at $t = 38$ s coincides with the triggering of the evaporation bolometer and marks the immediate removal of a part of the sample. The inset reveals that this removal takes about 0.5 s, consistent with Knudsen flow to the pump, impeded by the presence of the magnetic potential. To determine T and n_0, the three data points at each time step are fitted by Eq. (1), after filtering the raw data (time constant 0.5 s). The result is shown in Fig. 4. Also shown is the total number of particles N in the trap, related to n_0 and T through $N = n_0 V_{1e}$, where $V_{1e} \equiv \int n(\mathbf{r})/n_0 d\mathbf{r}$. For our trap the effective volume is well approximated by

$$V_{1e} = V_0 T^{5/2}(1 + 0.05\eta)[1 - 1.1\sqrt{\eta}(1 + 1.5\eta)e^{-\eta}], \tag{2}$$

where $V_0 = 72\ \mathrm{cm}^3\,\mathrm{K}^{-5/2}$ and $\eta \equiv \epsilon_{\mathrm{tr}}/k_B T$. The term between square brackets accounts for the influence on V_{1e} of the truncation of the distribution $n(\mathbf{r})$ at $B = B_w$. Initially the gas is in thermal equilibrium with the cell wall at $T \approx 0.2$ K and the density decays quickly due to a surface-induced mechanism. After triggering the bolometer T immediately drops to well below T_w. The resulting decrease of V_{1e} leads to an increase of n_0, in spite of the fact that particles are being removed.

To describe the evaporation quantitatively, we first discuss the relevant time scales. In thermal equilibrium, the average time τ_c between two elastic interatomic collision events is given by [2] $\tau_c^{-1} \approx 2^{5/2}\pi a^2 \bar{v} n_0 V_{2e}/V_{1e}$, where $a = 0.72$ Å is the s-wave scattering length, $\bar{v} = \sqrt{8k_BT/\pi m}$ is the average atomic speed, and $V_{2e}(T) \equiv V_{1e}(T/2)$. For $T = 0.2$ K and $n_0 = 1 \times 10^{11}\,\mathrm{cm}^{-3}$, $\tau_c \approx 10$ s. An atom on a trajectory intersecting the wall will undergo many wall collisions before meeting another atom, since the radial oscillation period $\tau_r \approx 0.4\,\mathrm{ms} \ll \tau_c$. The average time between two inelastic wall collisions $\tau_s \approx \tau_r/2s$, where s is the sticking probability, $s/T \approx 0.33\,\mathrm{K}^{-1}$ [12]. After sticking the H atoms desorb in a random direction and have on average a total energy $\epsilon_{\mathrm{tr}} + \frac{3}{2}k_B T_w$. These energetic atoms typically reach the trigger bolometer on a time scale $\tau_p \approx 0.5$ s.

In the temperature and density range considered, we have $\tau_s \ll \tau_p \ll \tau_c$. As a consequence, the evaporation proceeds in three stages. Immediately after triggering, the particles whose trajectories intersect the cell wall are removed instantly, leading to a nonequilibrium energy distribution. Subsequently, on a time scale of the order of τ_c, this distribution evolves towards a new equilibrium while simultaneously more particles evaporate as they scatter into wall-intersecting orbits. Finally the system will evolve in quasiequilibrium. We make no attempt to describe the nonequilibrium stage of the evaporation

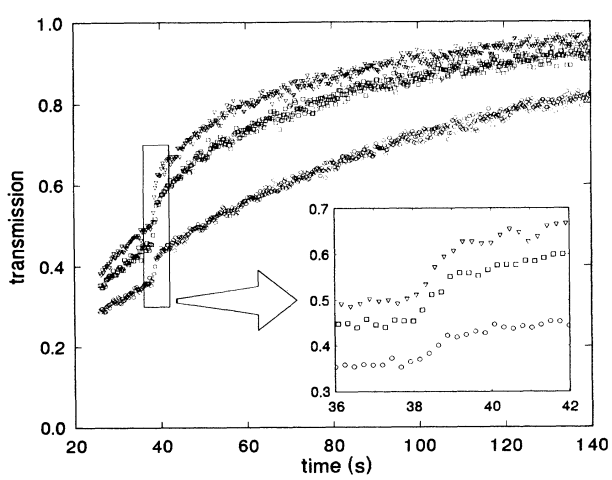

FIG. 3. Transmission vs time for three fixed frequencies (circles: $\nu - 0.48$ GHz; squares: $\nu + 0.48$ GHz; triangles: $\nu + 0.90$ GHz) in the blue wing of the σ_1 line. The jump at $t = 38$ s (inset) coincides with the triggering of evaporation.

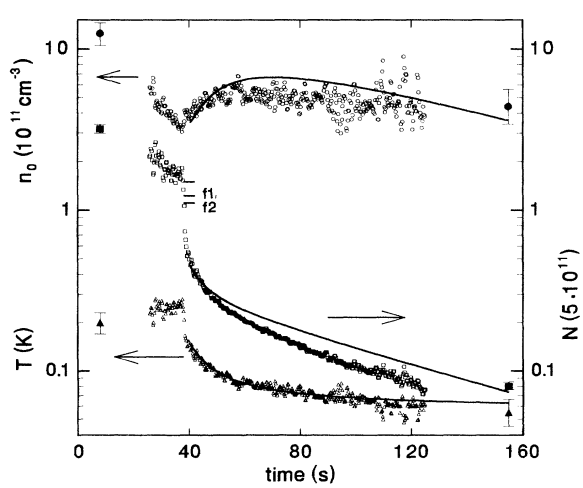

FIG. 4. T (triangles), n_0 (circles), and N (squares) vs time, calculated from the transmission data shown in Fig. 3. The isolated points at $t = 8$ s and 155 s are obtained from complete transmission spectra. The solid lines are the results of the evaporation model (see text).

process directly after the jump in N. In this period even the interpretation of the data is not unambiguous, as Eq. (1) was derived for thermal equilibrium.

To describe the initial jump in N and the evaporation rate in quasiequilibrium, we need an expression for the fraction f of particles in wall-intersecting orbits. The calculation of f is facilitated by the fact that the cell wall nearly coincides with the $B_w = 1.33$ T equipotential surface (note the difference in the horizontal and vertical scales in Fig. 1). We consider two limiting cases. First we assume that the axial angular momentum L_z is conserved between collisions, as would be the case for purely axially symmetric trapping potentials. This provides a lower bound f_1 for f. A straightforward calculation gives

$$f_1(\eta) = (V_{\rm geo}/V_{1e})\exp(-\eta), \tag{3}$$

where $V_{\rm geo} \approx 14\,{\rm cm}^3$ is the geometrical volume bounded by B_w. An upper bound f_2 is obtained by assuming that the small deviations from axial symmetry in our trapping field are sufficient to scramble L_z on a time scale τ_p. In this case f coincides with the fraction of atoms with total energy greater than $\epsilon_{\rm tr}$. We find for our trap

$$f_2(\eta) \approx (1.15 + 0.08\eta) f_1(\eta). \tag{4}$$

We assume that, when deviations from equilibrium are small, the rate at which atoms scatter into wall-intersecting orbits is given by $f\,c\,\tau_c^{-1}$, where c is a constant of order unity. The internal energy of the gas is given by $U_i \approx (\gamma + \frac{3}{2})Nk_BT$, where $\gamma \equiv \int U_p(\mathbf{r})n(\mathbf{r})d\mathbf{r}/Nk_BT = (T/V_{1e})dV_{1e}/dT$. If we equate $\dot{U}_i$ to the rate of energy change due to evaporation, we obtain the following set of coupled differential equations describing the evaporation dynamics:

$$\frac{\dot{N}}{N} = -f(\eta)\,c\,\tau_c^{-1} - \tau_1^{-1}, \tag{5}$$

$$\frac{\dot{\eta}}{\eta} = -\frac{\eta - \gamma}{\gamma + T(\partial\gamma/\partial T) + \frac{3}{2}} f(\eta)\,c\,\tau_c^{-1}. \tag{6}$$

Here, the phenomenological decay time τ_1 accounts for possible loss mechanisms, the nature of which we will discuss later. In view of the relatively low densities and short time scales, we neglected in Eqs. (5) and (6) any heating or particle loss due to the intrinsic dipolar decay [2]. Further, optical pumping to untrapped states (H$\downarrow$) does not occur on the σ_1 transition; it is suppressed for the other transitions by detuning and accounts for $\lesssim 1\%$ of the observed decay.

Using Eqs. (5), (6), and (2), we can apply the model to fit the experimental data for N, T, and n_0. The result obtained using $f(\eta) = f_2(\eta)$ is shown in Fig. 4 for $c = 0.9$ and $\tau_1 = 90$ s. In the fits, the first 2.5 s ($\approx \tau_c$) after the start of the evaporation were discarded for the reason discussed earlier. The curves obtained for $f(\eta) = f_1(\eta)$ are nearly identical but the resulting value for c is approximately 2 times higher. By evaluating f_1 and f_2 at the gas temperature just before triggering the evaporation, we calculate a lower (f_1N) and an upper bound (f_2N) for the initial jump in N, also indicated in Fig. 4. In view of the approximations made, the model is in reasonable agreement with the data.

Finally, we briefly comment on the possible origin of the observed decay mechanism of the evaporatively cooled gas. As mentioned before, τ_1 is much too short to be attributed to intrinsic dipolar decay. A wall-related spin relaxation would simply contribute to the evaporative cooling process and moreover would rapidly be halted as the gas cools to below the wall temperature. Decay mechanisms related to the incident light power were ruled out experimentally by temporarily blocking the L_α beam. The only remaining possibility seems to be collisions with He background gas, produced by room temperature radiation.

This research was supported by the Stichting voor Fundamenteel Onderzoek der Materie (FOM) and by the Nederlandse Organisatie voor Wetenschappelijk Onderzoek (NWO-PIONIER).

[1] H.F. Hess, G. Kochanski, J.M. Doyle, N. Masuhara, D. Kleppner, and T.J. Greytak, Phys. Rev. Lett. **59**, 672 (1987).

[2] R. van Roijen, J.J. Berkhout, S. Jaakkola, and J.T.M. Walraven, Phys. Rev. Lett. **61**, 931 (1988).

[3] N. Masuhara, J.M. Doyle, J.C. Sandberg, D. Kleppner, T.J. Greytak, H.F. Hess, and G.P. Kochanski, Phys. Rev. Lett. **61**, 935 (1988).

[4] J.M. Doyle, J.C. Sandberg, I.A. Yu, C.L. Cesar, D. Kleppner, and T.J. Greytak, Phys. Rev. Lett. **67**, 603 (1991).

[5] T.W. Hijmans, O.J. Luiten, I.D. Setija, and J.T.M. Walraven, J. Opt. Soc. Am. B **6**, 2235 (1989).

[6] K. Helmerson, A. Martin, and D.E. Pritchard, J. Opt. Soc. Am. B **9**, 483 (1992); **9**, 1988 (1992).

[7] A.L. Migdall, J.V. Prodan, W.D. Phillips, T.H. Bergemann, and H.J. Metcalf, Phys. Rev. Lett. **54**, 2596 (1985).

[8] For a collection of papers on optical cooling and trapping see J. Opt. Soc. Am. B **6** (1989).

[9] H.F. Hess, Phys. Rev. B **34**, 3476 (1986).

[10] A. Lagendijk, I.F. Silvera, and B.J. Verhaar, Phys. Rev. A **33**, 626 (1986).

[11] H.G.C. Werij, O.J. Luiten, I.D. Setija, T.W. Hijmans, and J.T.M. Walraven (to be published).

[12] J.J. Berkhout, E.J. Wolters, R. van Roijen, and J.T.M. Walraven, Phys. Rev. Lett. **57**, 2387 (1986).